Journal of Solid State Chemistry 182 (2009) 37–42

Contents lists available at ScienceDirect

Journal of Solid State Chemistry

journal homepage: www.elsevier.com/locate/jssc

Thin $La_2Zr_2O_7$ films made from a water-based solution

V. Cloet [a,*], J. Feys [a], R. Hühne [b], S. Hoste [a], I. Van Driessche [a]

[a] Ghent University, Krijgslaan 281–S3, 9000 Gent, Belgium
[b] Institute for Metallic Materials, IFW Dresden, Helmholtzstrasse 20, 01069 Dresden, Germany

ARTICLE INFO

Article history:
Received 3 June 2008
Received in revised form
26 August 2008
Accepted 31 August 2008
Available online 9 October 2008

Keywords:
Coated conductor
Sol–gel
$La_2Zr_2O_7$ films
Dip-coating

ABSTRACT

Thin films of $La_2Zr_2O_7$ (LZO) are highly regarded as possible buffer layers in the coated conductor configuration. This report describes a new synthesis for thin crystalline LZO films, based on a largely water-based solution, mainly containing metal acetates, acetic acid and an organic amine-base: triethanolamine. Initially, a thin layer of amorphous material is deposited on the textured Ni-5 at%W substrate by means of dip-coating. Only by careful control of the thermal treatment can the layer be transformed into a crystalline layer. Important parameters in this respect are the heating rate and the dwell time. The amorphous gel is analysed by HR-TGA/DTA and HR-TEM. The textured layers are analysed by XRD, pole figures, RHEED, AFM and SEM.

1. Introduction

So far, coated conductors possess the highest potential to solve the problems of up-scaling high temperature superconductor (such as $YBa_2Cu_3O_{7-x}$) applications. A coated conductor configuration addresses the two major problems of HTS: their brittle ceramic nature and the need for textured crystals. This configuration consists of a flexible metallic tape coated with thin protective films—called buffer layers—and finally coated with a thin film of YBCO. Ion beam assisted deposition (IBAD) and rolling assisted biaxially textured substrates (RABiTS) are the two most commonly used substrates, the latter being most promising for long-length production [1]. Potential materials for use as buffer layers need three distinctive qualities. First of all, the lattice parameter of the buffer layer must be similar to, or commensurate with, those of both substrate and YBCO. Only then can the buffer layers grow epitaxially on a textured substrate. Secondly, the thermal expansion coefficients of buffer layer and substrate must be comparable in order to avoid cracking and delamination during film growth. Finally, the buffer layer must act as an effective cation and/or oxygen diffusion barrier to prevent chemical interaction between adjacent materials. The most successful buffer layers reported so far are CeO_2, Y_2O_3-stabilised ZrO_2 (YSZ), Y_2O_3, MgO and $La_2Zr_2O_7$ (LZO) [2–4]. In order for this technology to be economically viable, the production costs must be as low as possible. The technique used for manufacturing these thin films will play a crucial role in achieving this goal. Vacuum techniques, which are expensive and difficult to up-scale, are therefore preferably avoided. An alternative technique that is being explored more often and applied with increasing success, is the chemical solution deposition (CSD) technique [5]. This technique does not require vacuum, has a higher deposition rate and uses widely accessible starting materials. Moreover, the composition of the solutions can be changed easily, which renders this method versatile. One of the implementations that is comprised under the general term CSD, is the sol–gel route. The starting sol(ution) can be transformed into a gel by heating at low temperatures ($<100\,^{\circ}C$) in ambient atmosphere. In the gel, all metal ions are homogeneously dispersed and prevented from precipitation by additives and pH adjustment [6].

This publication is concerned with the development and use of a water-based sol–gel route for the production of epitaxial LZO films on NiW-RABiTS tape. This method creates some additional advantages over the usually organic solvent-based CSD technique. Water is a safe, widely accessible, cheap and environmentally friendly solvent. Several coating techniques (dip-coating, spin-coating, ink-jet printing, etc.) can be applied to deposit the solution on the substrate [7,8]. This publication explores dip-coating of a sol–gel solution for the production of LZO thin films. Dip-coating allows the use of substrates of different geometries and sizes, coats both sides simultaneously and allows continuous processing in a reel-to-reel system.

* Corresponding author. Fax: +32 92 644 983.
E-mail address: veerle.cloet@ugent.be (V. Cloet).

0022-4596/$ - see front matter © 2008 Elsevier Inc. All rights reserved.
doi:10.1016/j.jssc.2008.08.031

2. Method

2.1. Precursor solution

The LZO solution was prepared by dissolving 1.6 g lanthanum (III) acetate hydrate ($La(CH_3COO)_3.1H_2O$, 99.9% Aldrich) in a mixture of 18 mL distilled water and 6.3 mL glacial acetic acid (CH_3COOH, 99.8%, Aldrich) at 90 °C. An equimolar quantity of zirconium (IV) hydroxide acetate hydrate ($Zr(OH)_3(CH_3COO).H_2O$, Aldrich) was added to this mixture, after all lanthanum acetate was dissolved. Upon cooling the solution to room temperature, triethanolamine ($N(CH_2CH_2OH)_3$, 99+%, Acros) was added. Finally, the acidity of the solution was decreased up to a value of 7 by adding ammonium hydroxide (25wt%, Chemlab). This procedure has been previously described in detail for the production of thin $YBa_2Cu_3O_7$-layers [9].

2.2. Substrate and coating

The Ni-5 at%W tape (evico GmbH, Germany) (80 μm thick) was cut into strips of approximately 2.5 cm length. Prior to dip-coating, the substrates needed cleaning to enhance wettability. In a first step these substrates were thermally cleaned at 800 °C (60 min) under Ar-5% H_2 atmosphere. After this, the substrates were chemically cleaned in different solvents. This cleaning procedure is described elsewhere in more detail [10]. The substrates were preserved in methanol to prevent degradation of the wettability and were used as soon as possible.

The substrates were dip-coated in a cupboard with a laminar flow classified as Class 10 according to the Federal Standard 209 and mounted in a Class 1000 clean room. The results presented here, were obtained after exploration of several variables such as dip-coat velocity, number of dip-coated layers, presence of seed layers. One could conclude that higher dip-coating velocities lead to thicker but less textured layers. In this research, in contrast to previous research [11], the presence of seed layers, did not improve the results. Therefore, the results of only one single layer, are discussed in this paper. A solution with a total metal concentration of 0.4 M was used for dip-coating. Dip-coating was carried out at room temperature with a dip-coat velocity of 20 mm/min and the substrates were withdrawn from the solution under an angle of 90°. The substrates were immersed in the solution for about 30 s before they were withdrawn. After deposition of the thin film, the substrate was dried in horizontal position at 60 °C for about 30 min. The colour change from opaque to yellow during gelation can be attributed to a colour change of the triethanolamine upon heating. A thermal treatment at high temperatures was needed to convert the amorphous gel to a crystalline textured film. The thin film was heated to 900 °C with a heating rate of 5 °C/min. After 50 min dwell time, the temperature was rapidly increased to 1050 °C and maintained constant for 50 min. This thermal treatment was carried out entirely under forming gas (Ar-5%H_2) atmosphere. The gas flow was kept constant at a value of 0.4 L/min. The sample was cooled to room temperature at a rate of 10 °C/min and under continuous flowing of forming gas.

2.3. Characterisation

The decomposition behaviour of the LZO gel was investigated by high resolution thermogravimetric analysis (TGA, TA-Instruments, Q500). An air flow on the sample of 60 mL/min was used. The maximal heating rate was 20 °C/min. Differential thermal analysis (DTA) was coupled to TGA to obtain information on physical changes that do not involve mass loss. Crystallinity and epitaxial growth of the films were investigated using standard X-ray diffraction. For acquiring θ–2θ-scans, a Siemens (D5000) was used. Pole figures, ω-scans and ϕ-scans were collected with a Bruker, AXS Discover. These measurements allow the determination of the full-width at half-maximum (FWHM) of the out-of-plane and the in-plane distribution of the oxide layer. Further analysis of the surface crystallinity was carried out by reflection high energy electron diffraction (RHEED, Staib Instruments). This technique allows analysis of the top 5 nm of the surface. An electron energy beam of 30 keV and a beam current of 50 μA was applied under a grazing incident angle (0.5–1.5°) to the sample. The diffraction pattern was recorded using a CCD camera and analysed with a computer program based on the kinematic theory of electron scattering. The surface microstructure was analysed with FEG–SEM (LEO 1530 Gemini) and its roughness by atomic force microscopy (AFM, molecular imaging, PicoPlus) in AC tapping mode. For transmission electron microscopic (TEM) analysis, a JEM 2200FS (JEOL) was used to obtain the images. Copper grids with mesh 2000 were immersed in the precursor solution and subsequently heated to the desired temperature under forming gas atmosphere.

3. Results and discussion

3.1. TGA–DTA

In order to obtain information about the decomposition behaviour of the gels and to adjust the thermal treatment accordingly, a TGA–DTA analysis of the gels was carried out. In Fig. 1 the TGA–DTA spectrum until 1000 °C is shown with an insert of a HR-TGA until 500 °C. At temperatures below 200 °C, two large decomposition steps occur in rapid succession. These two steps can be associated with the release of water, ammonia and acetic acid. These products are the main constituents of the gel and are most likely to evaporate quickly since their boiling point is lower than 200 °C. Soon after, at temperatures ranging from 200–500 °C, gases such as CO and CO_2 escape from the layer [12,13]. As can be seen from the thermogravimetric plot, there is no weight loss above 450 °C, only a small exothermic peak can be seen in the DTA curve at 780 °C. This corresponds most likely to the formation of LZO oxide out of La_2O_3 and ZrO_2. These findings are also confirmed by the TGA–DTA plots of lanthanum acetate and zirconium hydroxy acetate, in which it is clear that La_2O_3 and ZrO_2 are being formed at approximately 750 °C (not displayed here).

3.2. TEM

The transition from gel state to crystalline material is analysed by high resolution TEM of LZO powder. In Fig. 2, an overview of TEM micrographs of the gels at different temperatures is displayed. The dip-coated copper grids were heated to temperatures at which a weight loss was observed in the high resolution TGA. In this way, we can follow the behaviour of the gel and the transition into crystalline powder. Gels produced at low temperatures (60 °C) are unstable and quickly damaged by the electron beam, as the illuminated gel tends to blow up and burst open. Discrete particles are absent in the early gel stages until 305 °C. At 360 °C, small particles (10–50 nm) can be distinguished in the gel. At higher temperatures, larger particles form agglomerates. The particles formed at 820 °C are crystalline and have an average size of 30 nm. These findings are in good agreement with the conclusions drawn from the TG–DT analysis. Elemental analysis with electron energy-loss spectroscopy (EELS) will allow us to investigate the nature of the particles in the gels at 360 °C.

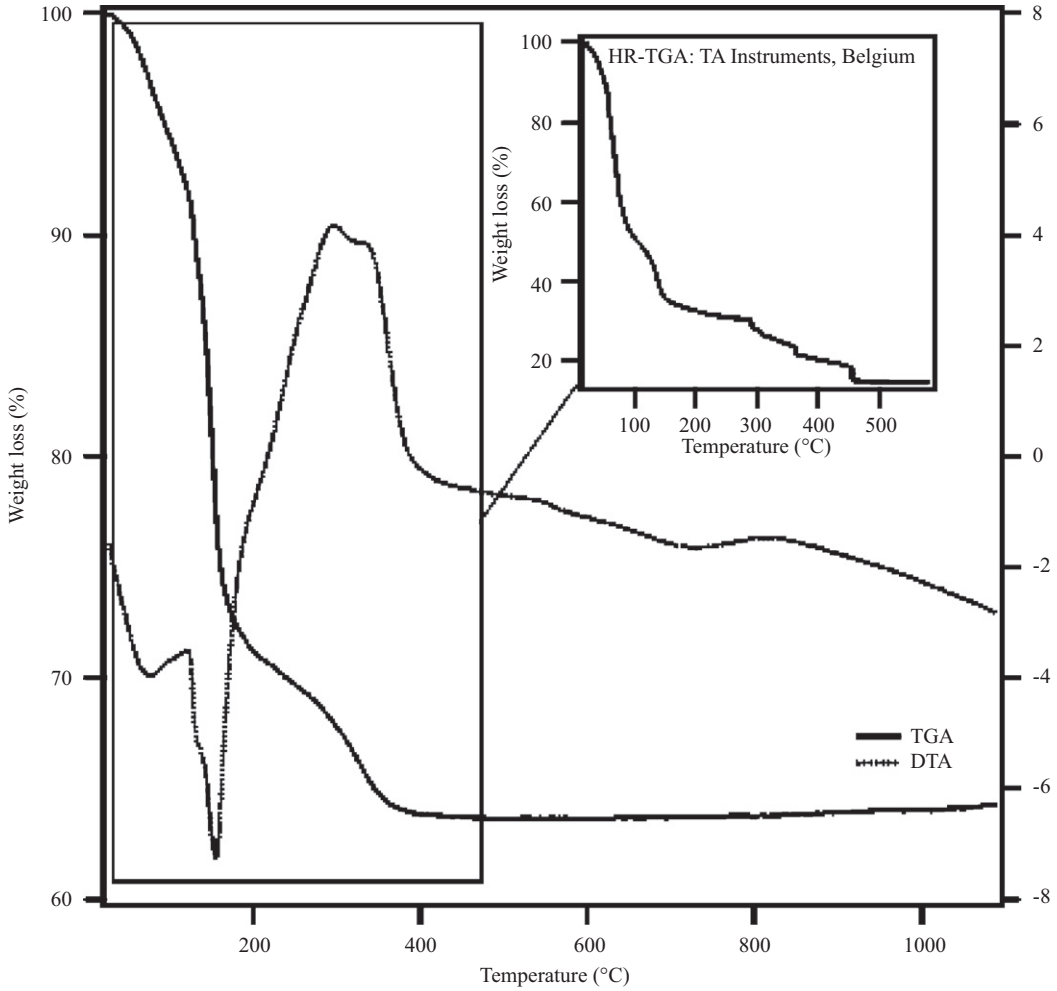

Fig. 1. HR-TGA of LZO gel.

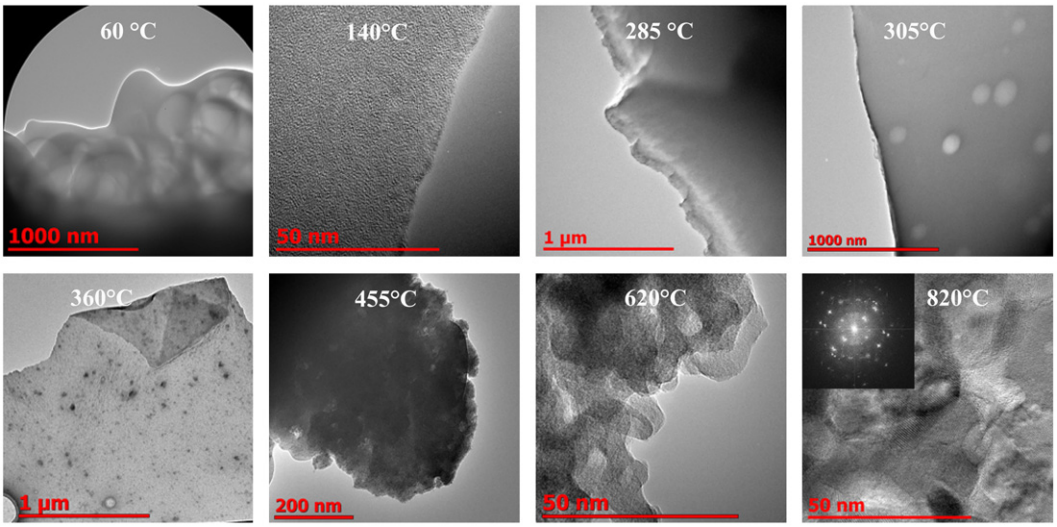

Fig. 2. TEM analysis of gel to solid phase transition.

3.3. XRD and RHEED

LZO has a cubic pyrochlore structure with a theoretical lattice parameter of 10.79 Å, which is in good agreement with the lattice parameter calculated from the (0 0 4) peak of the thin film (10.77 Å) and the one calculated from LZO bulk (10.79 Å). This lattice parameter results in a lattice mismatch of 0.5% and 1.8% with YBCO (resp. *a*- and *b*-axis). The lattice mismatch with the Ni-substrate is slightly higher (7.6%) but still allows the growth of epitaxial LZO. In Fig. 3 a θ–2θ scan of LZO–NiW is

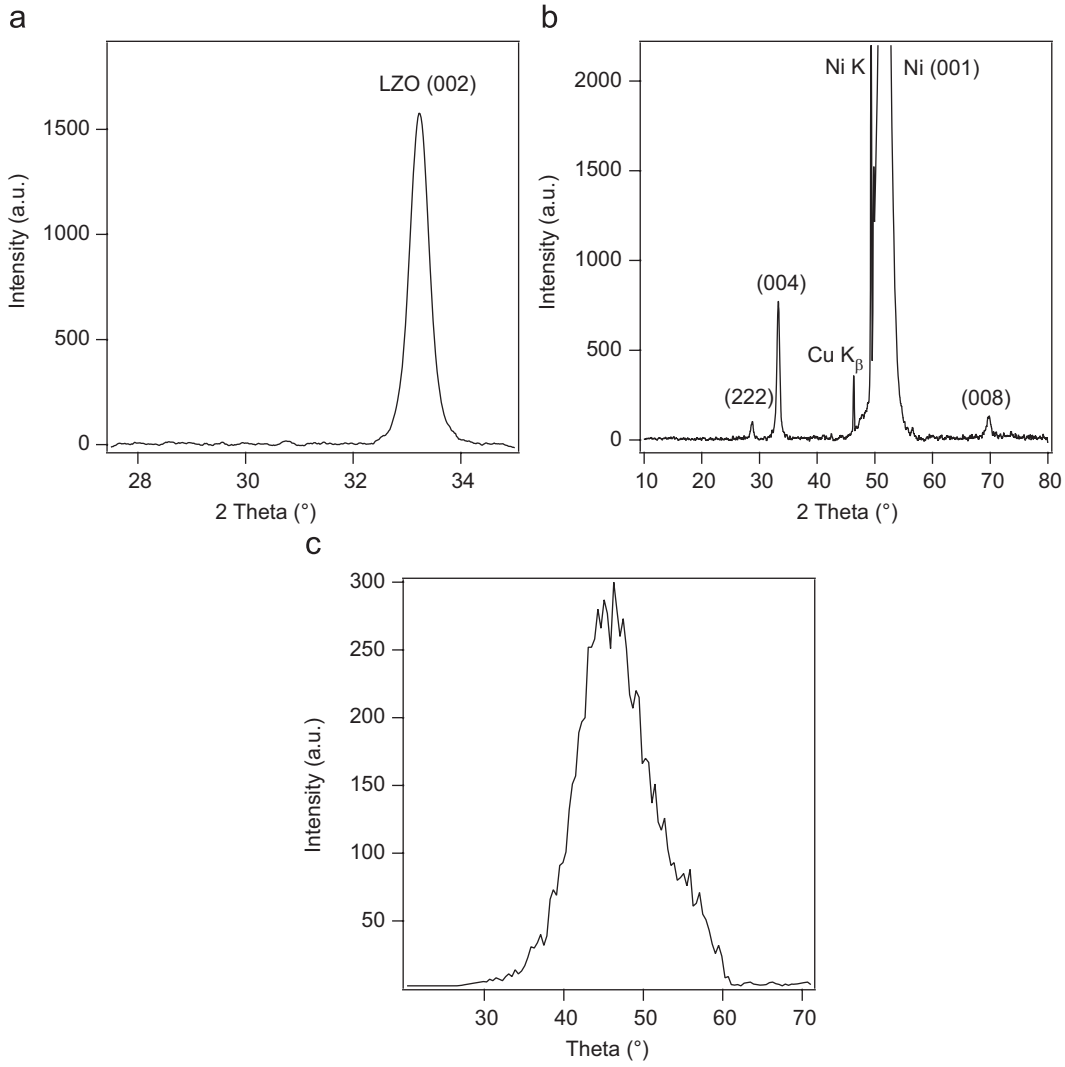

Fig. 3. Left: θ–2θ scan of LZO–NiW, right: rocking curve of (0 0 4) with FWHM = 8.8°.

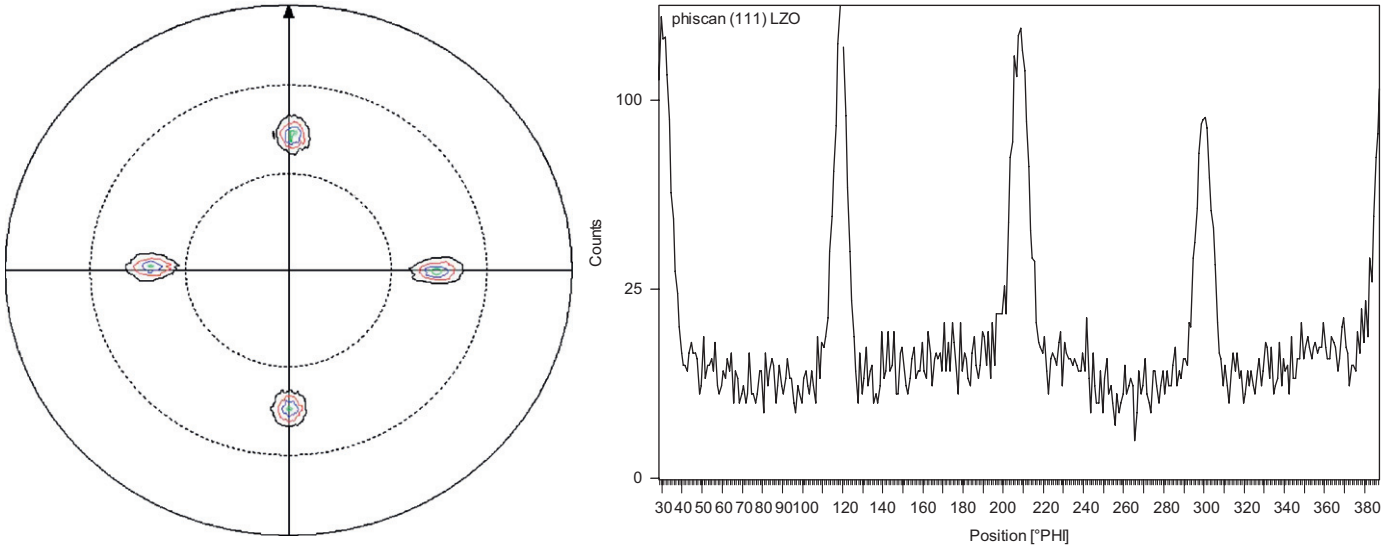

Fig. 4. Left: (2 2 2) pole figure of LZO, right: ϕ-scan of (2 2 2).

shown. As can be seen in this figure, only the (0 0 4) peak at $2\theta = 33.3^\circ$ is present. LZO has only two (0 0 l) reflections that can be observed in the range of 0–80° (Fig. 3b); the (0 0 4) orientation at $2\theta = 33.3^\circ$ and the less intense (0 0 8) orientation at $2\theta = 69.8^\circ$. This XRD spectrum dates from a previous sample and contains a small (1 1 1) peak. From Fig. 3a we can conclude that an epitaxial LZO layer is obtained as a result of the heat treatment described above. All *c*-axes of the LZO crystals are aligned perpendicular to the plane of the substrate. In this case, the (2 2 2) orientation (at $2\theta = 28.59^\circ$) has apparently been completely suppressed. The rocking curve of the (0 0 4) peak shows a FWHM of 8.8°. To check the in-plane misalignment of the thin film, (2 2 2) pole figures (at $2\theta = 28.6^\circ$) are taken. The FWHM of the peaks is 6.65° (Fig. 4).

For the epitaxial growth to be successful, the surface of the thin film must be well textured too. This can only be significantly measured with RHEED analysis. The highly energetic electrons used in RHEED analysis, penetrate only the top 5 nm which renders this technique surface sensitive. The pattern was indexed using a 10.6 Å lattice parameter for LZO. The RHEED pattern (Fig. 5) shows a well defined array of bright spots, which indicates that the top layer of the buffer layer is perfectly textured and crystalline. Therefore, we can conclude that the texture of the Ni-substrate was translated into a biaxial texture of the LZO buffer layer. The biaxial texture can in principle be passed on to the next layer.

3.4. SEM and AFM

The surface roughness, analysed by AFM, is given by the rms-value. In Fig. 6 the AFM micrograph is shown. Over an area of 25 μm^2, the rms-value is 11.3 nm and the average height is 42.2 nm. Upon omitting the large impurtity, the rms-value is further decreased to 8.66 nm and the average height is only 20.6 nm. These results give a better indication of the real surface morphology. In the SEM micrograph, at a magnification of 50 K, the small grains of LZO are visible. The overall surface of the LZO film is smooth and homogeneous.

3.5. Thin CeO_2 and $YBa_2Cu_3O_7$ films

In the final coated conductor structure, a thin film of CeO_2 and $YBa_2Cu_3O_7$ must be deposited on top of the LZO film. It is therefore important to test the compatibility of this LZO film with the following layers in reality. In this research, a 50 nm thick CeO_2 and a 300 nm thick YBCO layer are deposited by pulsed laser deposition (PLD) [14,15]. The peaks in the (1 1 1) pole figure

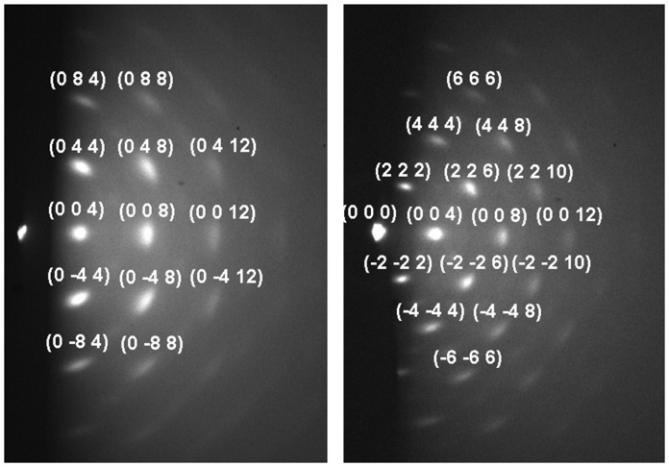

Fig. 5. RHEED pattern, view along the ⟨1 0 0⟩ and ⟨1 1 0⟩.

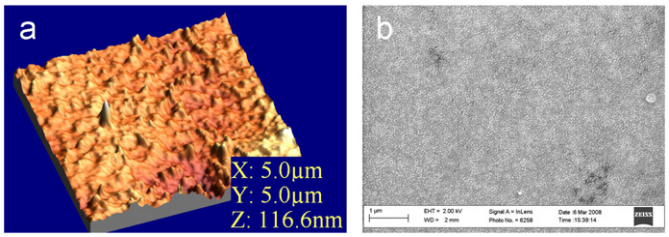

Fig. 6. Left: AFM micrograph, right: SEM micrograph at magnification = 50 K.

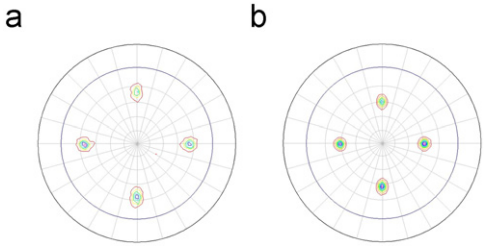

Fig. 7. Left: (1 1 1) pole figure of NiW/LZO/CeO_2, right: (1 0 3) pole figure of NiW/LZO/CeO_2/YBCO.

of LZO/CeO_2 have a FWHM of 9.1°. Comparing this to the 6.65° of Ni/LZO, we can conclude that the in-plane misorientation has increased a bit, but is still acceptable. For the actual superconducting layer, a (1 0 3) pole figure was taken and showed a FWHM of 8.7°. This shows the texture has been transfered successfully from the LZO layer up to the YBCO layer (Fig. 7).

4. Conclusion

The 0.4 M solution used in this research is composed of water, metal acetates, triethanolamine, acetic acid and ammonia and has been successfully used to produce epitaxial layers on NiW substrates. By applying a carefully chosen heat treatment, the growth of (2 2 2) oriented LZO crystals could be suppressed. The epitaxial films exhibit an out-of-plane FWHM of 8.8°. The in-plane orientation of the crystals can be linked to the FWHM of the (2 2 2) orientation, which is 6.65° and sufficiently small to deposit the next layer in the coated conductor configuration. The surface of the LZO layer was found to be smooth with only small inhomogeneities. TEM analysis of the gel state shows that until 360 °C the homogeneity of the gel is maintained and no precipitates are formed. At 360 °C, however, small inhomogeneities (15–50 nm) are found in the gel matrix. The finally obtained LZO solid grains have an average size of 30 nm and are found to be crystalline from 820 °C onwards. Further elemental analysis (electron energy-loss spectroscopy) of the inhomogeneities at 360 °C is under way to indicate whether these are small LZO nuclei or carbon residues. The PLD deposition of CeO_2 and YBCO showed that the biaxial texture could be maintained throughout the subsequent layers. A next step will be to deposit CeO_2 and YBCO by a similar sol–gel synthesis route as the LZO layer.

Acknowledgments

For realisation of XRD and pole figure analysis, the authors would like to thank Olivier Janssens (Ghent University, Belgium). For AFM analysis, the authors would like to thank Danny Vandeput (Ghent University, Belgium). The authors would also

like to thank Sebastian Engel (IFW, Dresden, Germany) for SEM analysis. For receiving Ni-W tapes, the authors would like to thank Trithor GmBH. One of us (V.C.) wish to thank the Institute for the Promotion of Innovation through Science and Technology in Flanders (IWT-Vlaanderen) for funding this research.

References

[1] J. Eickemeyer, D. Selbmann, R. Opitz, H. Wendrock, E. Maher, U. Miller, et al., Phys. C Superconductivity 372–376 (2002) 814–817.
[2] T.G. Chirayil, M. Paranthaman, D.B. Beach, D.F. Lee, A. Goyal, R.K. Williams, et al., Phys. C Superconductivity 336 (2000) 63–69.
[3] K. Knoth, R. Huhne, S. Oswald, L. Schultz, B. Holzapfel, Acta Materialia 55 (2007) 517–529.
[4] M.S. Bhuiyan, M. Paranthaman, K. Salama, Superconductor Sci. Technol. 19 (2006) R1–R21.
[5] M.S. Bhuiyan, M. Paranthaman, K. Salama, Superconductor Sci. Technol. 19 (2006) R1–R21.
[6] J. Livage, M. Henry, C. Sanchez, Prog. Solid State Chem. 18 (1988) 259–341.
[7] V. Cloet, M.C. Cordero-Cabrera, Adv. Sci. Technol. 47 (2006) 153–158.
[8] S. Morlens, L. Ortega, B. Rousseau, S. Phok, J.L. Deschanvre, P. Chaudouet, et al., Mater. Sci. Eng. B 104 (2003) 185–191.
[9] B. Schoofs, T. Mouganie, B.A. Glowacki, V. Cloet, S. Hoste, I. Van Driessche, J. Sol–Gel Sci. Technol. 41 (2007) 113–122.
[10] G. Penneman, I. Van Driessche, E. Bruneel, S. Hoste, Euro Ceram. Viii, Pts 1–3 264–268 (2004) 501–504.
[11] X.B. Zhu, L. Chen, S.M. Liu, W.H. Song, Y.P. Sun, K. Shi, et al., Phys. C Superconductivity 415 (2004) 57–61.
[12] L. Fabbrini, I. Rossetti, L. Forni, Appl. Catal. B Environ. 56 (2005) 221–227.
[13] G. Hussein, J. Therm. Anal. Calorimetry 42 (1994) 1091–1102.
[14] S. Engel, K. Knoth, R. Huhne, L. Schultz, B. Holzapfel, Superconductor Sci. Technol. 18 (2005) 1385–1390.
[15] M.A. Arranz, B. Holzapfel, N. Reger, J. Eickemeyer, L. Schultz, Phys. C Superconductivity 366 (2002) 109–116.